Biochemistry

 Volume 41, Number 23 June 11, 2002

Accelerated Publications

Vibration Spectroscopy Reveals Light-Induced Chromophore and Protein Structural Changes in the LOV2 Domain of the Plant Blue-Light Receptor Phototropin 1†

Trevor E. Swartz,‡ Phillip J. Wenzel,§ Stephanie B. Corchnoy,§ Winslow R. Briggs,‡ and Roberto A. Bogomolni*,§

Department of Chemistry and Biochemistry, University of California, Santa Cruz, California 95064, and Department of Plant Biology, Carnegie Institution of Washington, Stanford, California 94305

Received March 25, 2002; Revised Manuscript Received April 22, 2002

ABSTRACT: Phototropins (phot1 and phot2), the plant blue-light receptors for phototropism, chloroplast movement, and stomatal opening, are flavoproteins that contain two ~12 kDa FMN-binding domains, LOV1 and LOV2, at their N-terminus, and a serine/threonine protein kinase domain at their C-terminus. The light-activated LOV2 domain forms a metastable intermediate which has been shown to be a protein−chromophore cysteinyl adduct (Cys39) at C(4a) of FMN. This species thermally relaxes back to the ground state in the dark. We measured the light-minus-dark FTIR difference spectra for the LOV2 domain of oat phot1. These spectra show the disappearance of bands at 1580, 1550, and 1350 cm^{-1} that originate from, or are strongly coupled to, the N5═C(4a) stretching vibrations, consistent with the perturbations expected upon C(4a) adduct formation. Assignment of these negative difference FTIR bands to native chromophore vibrations is based on the alignment with resonance Raman bands of FMN. Prominent positive bands include a doublet at 1516 and 1536 cm^{-1} and one at 1375 and 1298 cm^{-1}. Normal-mode vibrational-frequency calculations for both lumiflavin and lumiflavin with a sulfur attached at the C(4a) position agree with many of the positive and negative bands observed in the difference spectra. Both calculated and experimental difference FTIR spectra for deuterium isotope substitutions at exchangeable positions in the flavin chromophore are consistent with the assignment of the above positive bands to vibrational modes involving both the newly formed tetrahedral geometry of C(4a) and the N5−H bond in the long-lived $LOV2^{S}_{390}$ cysteinyl species.

Phot1 and phot2 (formerly nph1 and npl1, respectively) belong to the recently discovered phototropin family of blue-light receptors in higher plants (*1*, *2*). Phot1 and phot2 mediate diverse physiological responses to blue light in plants, including phototropism, chloroplast relocation, and stomatal opening (*3*−*7*). Phot1 and phot2 are homologous flavoproteins; they both contain two LOV domains [the LOV domains are a family of proteins that are regulated by light, oxygen, and voltage and belong to the (PAS) PER/ARNT/SIM superfamily (*8*)] and a typical serine/threonine kinase at the C-terminus (*2*). Each LOV domain binds an FMN[1] chromophore noncovalently (*9*). Following blue-light activation, the LOV domains expressed in *Escherichia coli* undergo

† This work was supported by NSF Grant DMB-0090817 (R.A.B.) and NSF Grants IBN9601164 and MCB0091384 (W.R.B.).

* To whom correspondence should be addressed: Department of Chemistry and Biochemistry, University of California, 1156 High St., Santa Cruz, CA 95064. Telephone: (831) 459-4294. Fax: (831) 459-2935. E-mail: bogo@chemistry.ucsc.edu.

‡ Carnegie Institution of Washington.

§ University of California.

[1] Abbreviation: FMN, flavin mononucleotide.

10.1021/bi025861u CCC: $22.00
Published on Web 05/17/2002

Scheme 1: Simplified Photocycle for LOV2[a]

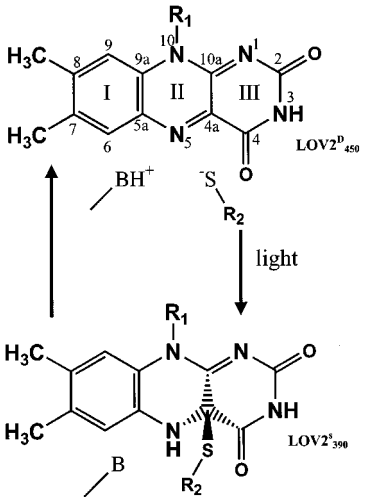

[a] R_1 represents the ribityl side chain of FMN. Normal-mode calculations were conducted on lumiflavin ($R_1 = CH'_3$). LOV^S_{390} shows the chromophore rearrangement following illumination. For normal-mode calculations of the adduct species, $R_1 = CH'_3$ and $R_2 = H$. In $LOV2^S_{390}$, R_2 is cysteine 39 and connects FMN to the protein. Note that upon adduct formation, C(4a) converts from sp^2 to sp^3 hybridization, resulting in puckering of FMN between ring II and ring III.

a cyclic photoreaction, in which the primary photoproduct returns spontaneously in the dark to the ground state (*10*, *11*).

The early steps of the LOV2 photocycle involve decay from the excited singlet state of the FMN chromophore into a triplet state in an as yet unresolved time, presumably on the sub-nanosecond time scale (*11*). The triplet state acts as the molecular switch that drives the photochemical reaction (*11*), as decay to the triplet state involves a redistribution of the electronic densities that significantly increases the pK_a of N5 of FMN (*12*). This increase in basicity results in protonation of N5, presumably from a neighboring protein side chain donor, and loss of the FMN N5═C(4a) double bond, causing C(4a) to become a (positively charged) reactive carbocation. The cysteine 39 sulfur atom, which is approximately 4.2 Å from C(4a), attacks the carbocation, resulting in the formation of a protein−FMN adduct (*11*, *13*). This adduct is a long-lived intermediate and has been labeled $LOV2^S_{390}$; the 390 signifies maximum absorption at 390 nm, and the S signifies its tentative assignment as a cellular signaling state of the protein (*11*). The $LOV2^S_{390}$ cysteinyl−flavin adduct breaks down spontaneously, and the system returns to the ground state following a first-order, thermally activated reaction with a half-life of ∼50 s at 20 °C (Scheme 1).

For phot1, both LOV1 and LOV2 undergo similar photocycles (*11*); the quantum efficiency of LOV1 is much lower (about $^1/_{10}$) than that of LOV2 (*10*). Studies of phot2 show absorption spectra of LOV1 and LOV2 ground states and respective long-lived intermediates that are similar to those of phot1, suggesting a similar underlying photocycle mechanism (*5*). The respective quantum yields and reaction rates for the LOV domains of phot2 differ from those of the LOV domains in phot1 (*14*).

The ground state of LOV2 absorbs maximally at 450 nm ($LOV2^D_{450}$), with vibronic bands at 425 and 475 nm; in addition, there are chromophore absorption bands at 370 and 270 nm. Formation of the adduct results in a loss of the blue absorption band, leaving an absorption band centered at 390 nm. The early assignment of the long-lived photoproduct as an FMN−protein adduct was based on the similarities in the absorption spectrum of $LOV2^S_{390}$ to that of a mutant mercuric reductase enzyme that had been postulated to include such an adduct in its reaction mechanism (*15*). The site-specific mutant LOV2-Cys39Ala provided evidence that Cys39 is the protein residue involved in the reaction (*10*). This adduct assignment has been confirmed by both NMR and X-ray crystallography (*16*, *17*). We present here the first evidence using vibration spectroscopy for the formation of a protein−C(4a)FMN adduct in the phot1−$LOV2^S_{390}$ photocycle intermediate. Both ground state and $LOV2^S_{390}$ chromophore bands are assigned in the difference FTIR absorption spectrum presented here. In addition, the difference spectrum shows numerous positive and negative bands that may reflect protein backbone and/or protein side chain conformation changes.

EXPERIMENTAL PROCEDURES

Oat phot1 LOV2 protein was expressed in *E. coli* and purified as described previously (*11*, *16*). Salt and buffer concentrations in samples were adjusted by repeatedly concentrating (Continental Lab Products, San Diego, CA) and resuspending in 5 mM Tris and 10 mM NaCl (pH 8). The final sample containing 1.7 mg of protein (calculated from the LOV2 extinction coefficient) was lyophilized and resuspended in 120 μL of either H_2O or D_2O (Sigma). The sample (20 μL) was then placed on an AgCl window (International Crystal Labs, Garfield, NJ), and the solvent was partially evaporated by a slow flow of dry nitrogen. The wet sample was then sandwiched between a second AgCl window and placed in the spectrometer. A similar procedure has been used to yield photochemically competent PYP (*18*).

Transmission FTIR was performed on a Nicolet 800 (Madison, WI) spectrometer equipped with a liquid nitrogen-cooled MCT detector. Each data set included an average of 1064 scans (∼6 min). Blue-light illumination of the sample in the FTIR compartment was provided by a Zeiss 30W tungsten filament illumination system. The light beam was passed through a filter set [800 nm short-pass filter, a Corning 3-37 filter, a Corning 4-96 filter, and a Corion 80 nm bandpass interference filter (λ_{max} = 420 nm), with a final bandpass of ∼80 nm centered around 430 nm] and focused onto the sample inside the FTIR spectrometer sample compartment through a plexiglass window. The light-minus-dark difference spectrum was obtained by subtraction of a spectrum collected in the dark from a second spectrum collected while continuously illuminating the sample. To maximize the fraction converted into the $LOV2^S_{390}$ form, we illuminated the sample for at least 30 s prior to data collection. Following irradiation, a second dark spectrum was collected after several minutes to confirm that the sample had fully relaxed into its ground state and was therefore photochemically active. Fourier transforms of interferograms and analysis of spectra were carried out with a personal computer (PC) using GRAMS/32 (Galactic Industries).

Raman spectra were collected using a system of our own construction with a typical 90° geometry for sample illumination and scattered light collection (*19*). A 514.7 nm

Table 1: Assignment of Bands for the Adduct Model Compound[a]

band	frequency range (cm^{-1})	intensity	D shift	assignment
I	1717−1788	vs	n	C2═O, C4═O symmetric stretching, N10−C(10a) stretch
II	1710−1780	vs	− −	C4═O stretch antisymmetric with C2═O stretch, strong N3−H bend
III	1582−1647	s	n	ring I stretch, C(10a)−N1 stretch
IV	1541−1604	vs	n	ring I stretch, C(10a)−N1 stretch antisymmetric with C(5a)−C(9a) stretch, some N5−H bend
V	1537−1601	vs	−	ring I stretch, C(10a)−N1 stretch symmetric with C(5a)−C(9a) stretch, some N5−H bend
VI	1471−1531	w	n	ring I stretch, C6−H, C9−H bend, weak N5−H bend
VII	1456−1516	w	−	ring I stretch, N5−H bend, methyl deformation
VIII	1383−1440	w	n	C′ methyl deformation, ring I, II, and III motion
IX	1363−1419	s	− −	ring I, II, and III stretch, N5−H bend
XI	1302−1356	s	− − −	N3−H bend, some ring I deformation
XII	1267−1319	vs	n	ring I, II, and III stretch
XIII	1196−1245	s	−	N5−C(4a) stretch, ring I deformation
XIV	1143−1190	s	−	C2−N3 stretch, N3−H bend, C(4a)−N5 stretch
XV	1029−1071	w	n	ring I deformation, C(4a)−C4 stretch

[a] Results from normal-mode frequency calculations for a model adduct. Predicted frequencies are shown as a range (see the text). Frequency shifts expected for H−D exchange at both the N3−H and N5−H groups of the model compound (see Scheme 1); a minus (−) sign indicates a predicted shift to lower wavenumber, and the number of minus signs indicates the magnitude of the shift. n indicates negligible shift, vs very strong, s strong, and w weak.

argon ion laser beam (model 164, Spectra Physics) was focused onto the sample by a spherical lens. Raman scattered light was collected with a Bausch & Lomb quartz lens condenser system ($f = 1.7$) that produced a collimated beam that a second lens ($f = 10$) focused on the entrance slit of a Spex (Metuchen, NJ) 1870 0.5 m single-grating spectrograph. Raleigh scattered laser light was removed by two high-pass 3-75 Corning glass filters (cutoff wavelength of ∼530 nm). A Spex grating with 2.7 nm/mm dispersion allowed for collection of a 40 nm spectrum at its exit focal plane by an EG&G optical multichannel analyzer (OMA) III 512 diode array. At the 514 nm laser probe wavelength, this represents a 1200 cm^{-1} spectral window, covering the full spectral range of interest in one pass. At the typical entrance slit aperture that was used (0.1 mm), the resolution of the system was ∼4 cm^{-1}. We corrected for the spectral response of the entire detection system (lens, filters, spectrograph, and diode gain) by using a calibrated white light source from a halogen lamp (3400 K). A solution containing 1 mM FMN (Sigma) and 6 M KI was sealed in a 3 mm glass capillary tube for Raman collection. Data were transferred from the OMA to a PC for analysis using GRAMS/32.

Light-induced absorbance difference spectra in the visible region were collected on the same sample used in the FTIR experiments. The FTIR sample holder with the sample in place was mounted in the sample compartment of an HP8452a diode array spectrophotometer and illuminated as described above for the FTIR measurements. The spectrophotometer was controlled by programs written in Labview, and data analysis was carried out using Matlab routines as described previously (*11*).

Normal-mode frequency calculations were performed using density function theory (DFT). We used the B3-LYP method with a 6-31G(d) basis set. All calculations were run with Gaussian98 (*20*). The geometry of the model compound was first optimized by analytic gradient techniques. A scaling factor of 0.9614 was applied to the resulting frequencies. This scaling factor had previously been shown to predict B3LYP/6-31G(d) frequencies in which ∼80% of assigned values fall within 4% of observed values, with a root-mean-square deviation of 34 cm^{-1} (*21*). To assign our experimental data correctly to bands predicted by calculations (after appropriate scaling), we assume experimental bands fall within ±2% of those predicted by calculations. This uncertainty in calculations is reflected in the frequency ranges presented in Table 1, with the majority of experimentally observed modes falling to the center of the frequency ranges that are presented.

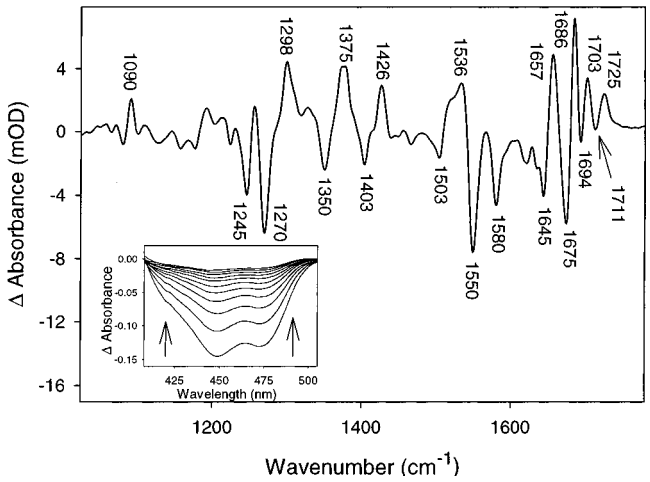

FIGURE 1: Difference between the FTIR spectra of $LOV2^{S}_{390}$ and $LOV2^{D}_{450}$. Prominent bands assigned to $LOV2^{S}_{390}$ (positive bands) and $LOV2^{D}_{450}$ (negative bands) are labeled. The inset shows light-minus-dark difference spectra of LOV2 mounted in the FTIR sample holder (see the text). Difference spectra during spontaneous thermal decay of $LOV2^{S}_{390}$ were collected every 10 s after illumination. The rate of recovery of ground state $LOV2^{D}_{450}$ from $LOV2^{S}_{390}$ is consistent with previously reported relaxation rates (*10*, *11*). Arrows indicate the course of recovery in the dark.

RESULTS AND DISCUSSION

Photochemistry of Rehydrated LOV2 Mounted onto IR Supports. Rehydration, and partial aqueous solvent evaporation necessary during the sample mounting, produced IR samples with slightly higher buffer and salt concentrations than the original aqueous LOV2 stock solutions. These rehydrated and mounted samples show photochemical activity consistent with that previously reported for samples in aqueous solution (*10*, *11*). The inset of Figure 1 shows the light-induced absorbance changes of a typical sample mounted in the IR sandwich cell used for the FTIR work. Because of the transmission properties of the IR windows,

the data were restricted to the visible region of the spectrum. The dark-regeneration half-life was 30 s at room temperature and pH 8, and the final sample absorbance at 450 nm mounted in the IR cell was approximately 0.2 absorbance unit. The maximal absorbance change observed indicates that a large fraction of the sample is photoconverted to $LOV2^{S}_{390}$ by the actinic light source.

Light-Induced FTIR Absorbance Changes of LOV2. Figure 1 shows the difference in IR absorption between the light-generated $LOV2^{S}_{390}$ state and the ground state of the chromoprotein, $LOV2^{D}_{450}$. This light-minus-dark difference FTIR absorbance spectrum shows numerous positive and negative bands that result from differences in IR absorption of both chromophore and protein moieties. Negative bands are usually attributed to vibrational transitions of the ground state that either have been shifted to other frequencies or have been entirely bleached as a consequence of the photochemical reaction, whereas positive bands are assigned to the light-generated state (*22*). In Figure 1, we label the most prominent negative and positive difference FTIR vibrational bands. To assign chromophore vibrational bands, we utilized a combination of techniques, including resonance Raman spectroscopy, deuterium exchange, and normal-mode calculations.

Vibrational transition frequencies that can be attributed exclusively to the chromophore can be identified in the complex difference spectrum using resonance Raman spectroscopy, where Raman scattering is probed at laser frequencies close to the electronic absorption maximum of the chromophore (resonance region). At resonance, chromophore scattering bands are enhanced in intensity by several orders of magnitude over those off-resonance bands of protein and/or other nonabsorbing components of the molecule, effectively making all observable bands originate from chromophore vibrations. LOV2 in fairly dilute ($<10^{-4}$ M) samples is stable, but the chromophore fluorescence is more intense than the Raman scattered radiation by orders of magnitude at laser probe wavelengths needed to acquire resonance Raman spectra.

It has been observed that the resonance (or preresonance) Raman spectra of many nonfluorescent flavin-binding proteins exhibit vibrational frequencies nearly identical to those of isolated FMN (or other isoalloxazine) chromophores in solution (*19*). This has recently been shown to be the case for *Chlamydomonas* phot LOV1 (*23*). In all cases, the isoalloxazine chromophores are noncovalently bound to the proteins (*19*), as is the case in LOV2 (*9*, *13*). We therefore aligned an FMN resonance Raman spectrum with the LOV2 difference FTIR spectrum to identify FTIR vibrational frequencies of the FMN chromophore's ground state. We measured the FMN resonance Raman spectrum using the 514 nm argon ion line as a probe in the presence of 6 M KI to quench the fluorescence.

As can be seen in Figure 2, many of the negative bands in the difference IR spectrum line up well with the resonance Raman spectrum of FMN and may thus be assigned to the chromophore ground state (*19*). Specifically, negative FTIR bands at 1711, 1580, 1550, 1503, 1350, 1270, and 1245 cm^{-1} are in good agreement with those previously assigned to the isoalloxazine structure by a combination of resonance Raman on native and isotopically labeled FMN and normal-mode calculations (*24*−*27*).

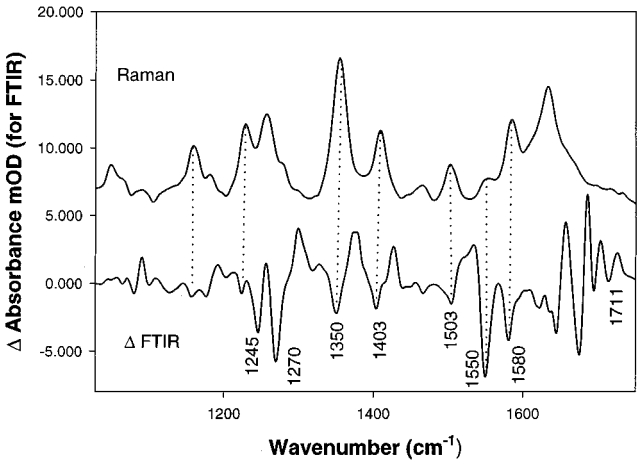

FIGURE 2: Difference between the FTIR spectra of $LOV2^{S}_{390}$ and $LOV2^{D}_{450}$ aligned with resonance Raman spectra of FMN. Alignment of negative difference FTIR bands with FMN bands indicates LOV2 chromophore bands that undergo perturbation during the photocycle.

Light Activation of LOV2 Results in Conversion of the FMN N5═C(4a) Double Bond to a Single Bond. Motions of the C(4a) atom contribute to nearly all normal-mode vibrations of FMN because of the atom's central position in the molecule (*25*). However, some vibrational modes predominantly involve motion of C(4a). Two bands that are very strongly coupled to C(4a) vibrations are at 1580 and 1550 cm^{-1}. Both of these modes show a large shift in resonance Raman experiments using isotopically labeled ^{13}C(4a) (*28*), with the 1580 and 1550 cm^{-1} bands shifting by 8 and 5 cm^{-1}, respectively. Both modes involve C(4a)═N5 stretching (see Scheme 1 for FMN numbering). This was confirmed by shifts caused by isotopic substitution of ^{15}N5 (*28*). The 1580 cm^{-1} mode also involves a significant contribution of C(10a)═N1 stretching that is out of phase with the C(4a)═N5 stretching. Thus, this mode strongly involves N5═C(4a)−C(10a)═N1 conjugation (*26*). The 1550 cm^{-1} band also involves a similar conjugation (*26*); the difference is that the 1580 cm^{-1} band has the C(4a)═N5 stretch in phase with the C(10a)═N1 stretch, whereas the 1550 cm^{-1} band has these two stretches out of phase (*25*). These bands are therefore expected to be greatly affected upon adduct formation in LOV2 because the protein−flavin adduct would change C(4a) from a planar carbon (sp^2) to a tetrahedral carbon (sp^3), with disappearance of the C(4a)═N5 double bond and formation of a C(4a)−N5 single bond. On adduct formation, these modes no longer exist and hence result in negative peaks in the FTIR difference spectra.

The shifts of some of the normal-mode frequencies of free FMN caused by D/H substitution of the N3−H group have been previously assigned by resonance Raman spectroscopy of isotopically substituted compounds and normal-mode calculations (*27*). Deuterium isotope exchange of the N3 proton can also be used in the assignments of vibrational frequencies to normal modes of protein-bound FMN when exchange is possible. We have previously shown that the N3 proton readily exchanges with bulk protons (*11*). Neither the 1580 nor the 1550 cm^{-1} mode involves significant motions of the N3 proton; they are expected to show negligible shifts upon D/H exchange (*27*). In LOV2, the very small effect of deuterium substitution on the 1580 and 1550 cm^{-1} bands shown in Figure 3A is consistent with the above

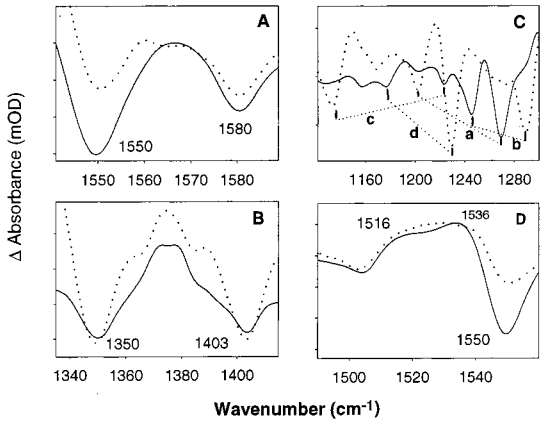

FIGURE 3: (A−D) Difference between the FTIR spectra of $LOV2^{S}_{390}$ and $LOV2^{D}_{450}$ for selected regions of the spectra. Solid lines represent spectra for LOV2 in H_2O, and dotted lines represent spectra for LOV2 in D_2O. Labeled negative bands are assigned to FMN modes that have previously been identified with their corresponding D_2O shifts. In panels A and B, negative bands show negligible shifts; panel C shows major shifts upon H/D exchange in the N3−H group, with corresponding modes of negative peaks diagrammed with connecting lines. The corresponding shifts are (a) from 1270 to 1202 cm^{-1}, (b) from 1245 to 1290 cm^{-1}, (c) from 1223 to 1133 cm^{-1}, and (d) from 1176 to 1228 cm^{-1}. See the text for a discussion of relative shifts of modes. In panel D, two positive bands at 1536 and 1516 cm^{-1} are assigned to modes that arise upon formation of an adduct at C(4a). Nominal shifts of these bands upon H/D exchange in the N3−H and N5−H groups are predicted by normal-mode calculations (see the text).

assignments. The 1503 cm^{-1} band, which mostly involves CH_3 deformation, does not shift upon D/H exchange as is expected (*27*). Other negative bands that align with known FMN bands also show good correspondence with established frequency shifts caused by deuterium exchange of the N3 proton.

Panels B and C of Figure 3 compare FTIR difference spectra of LOV2 in both H_2O and D_2O in the 1100−1420 cm^{-1} range. Figure 3B shows that the spectral shift for both the 1403 and 1350 cm^{-1} bands is very small, consistent with previous observations. Both bands are dominated by ring stretching vibrations and some methyl group deformations (*27*). The 1100−1300 cm^{-1} region of the spectrum shows a complex pattern of significant shifts upon N3 deuteration. Many of these bands have been previously assigned to modes that involve movements of the N3 proton (*27*). The D/H exchange frequency shifts in LOV2 shown in Figure 3C fit well with the D/H shifts previously assigned in N3 D/H-substituted riboflavin (*27*). We indicate these correlated modes with connecting lines in Figure 3C. The 1270 cm^{-1} band involves bending motions of the N3−H group and is expected, and observed, to shift to lower frequencies around 1202 cm^{-1}. The 1245 cm^{-1} mode has contributions made by stretchings of the C(9a)−N10 and C6−N1 bonds and bending of the N3−H bond, both C═O groups, the C5−H group, and the C6−H group, and is expected and found to shift to higher frequencies around 1290 cm^{-1}. Also consistent with earlier assignments, the 1223 cm^{-1} mode that involves mainly N3−C4 and C8−CH_3 stretching shifts to a lower frequency around 1133 cm^{-1}, and the 1176 cm^{-1} band that involves N1−C2, C2−N3, N3−C4, C4−C(4a), C(4a)−C(10a), and C7−CH_3 stretching modes shifts to a higher frequency around 1228 cm^{-1}. All of these observations and assignments of negative bands are consistent with changes in the IR spectrum expected from the loss of the N5═C(4a) double bond upon formation of a cysteinyl−flavin adduct. In addition, we have tentatively assigned positive bands at 1536 and 1516 cm^{-1} specifically to stretching vibrations of the newly formed sp^3 carbon (see below).

Normal-Mode Harmonic Vibrational Calculation for a Model Flavin S−C(4a) Adduct. The interpretation and band assignments of vibrational spectra rely strongly on supporting evidence from theoretical calculations of vibrational-mode frequencies of applicable model systems. Normal-mode calculations for lumiflavin and other flavin chromophores have been reported and used in the assignment of vibrational spectroscopy data in numerous flavins and flavoproteins (*25*, *26*, *29*) and extended here to interpret the LOV2 negative FTIR bands. Assignment of the positive bands requires knowledge of vibrational frequencies for the $LOV2^{S}_{390}$ flavin product, which has been proposed to be a protein/flavin S−C(4a) adduct. We did not find in the literature normal-mode analysis of C(4a) flavin adducts. Therefore, we performed harmonic frequency calculations on a flavin model compound that has a thiol adduct at position C(4a) (see Scheme 1). As a control, we performed normal-mode frequency calculations for lumiflavin and attained results consistent with those reported previously (*29*). Our model compound has 34 atoms and therefore shows 96 normal modes. We show in Table 1 only bands with at least moderate intensity that fall within our experimental frequency range. They are labeled with Roman numerals for the purpose of discussion; we also list their calculated frequencies, their relative strengths for the model adduct containing hydrogens at positions N3 and N5, and the calculated frequency shifts when these hydrogens are substituted with deuteriums. As expected, larger deuterium shifts accompany modes that involve bending vibrations of the N3−H and/or N5−H group. These frequencies and intensities apply to lumiflavin model compounds in a homogeneous dielectric environment. The protein environment is expected to be anisotropic. Furthermore, numerous interactions, particularly hydrogen bonding involving carbonyls and N−H groups (*27*), may alter slightly the intensities, frequencies, and deuterium shifts of vibrations coupled to the motions of these atoms (*27*). We note that most experimental frequencies that we assigned on the basis of intensities and deuterium shifts to vibrational modes coupled to motion of hydrogen bonding atoms are consistently shifted to lower frequencies with respect to the values calculated for the isolated chromophore. The S−C bond vibrations in the adduct are predicted to be in the low (<1000 cm^{-1}) range, but we cannot identify those bands unambiguously at this time without specific isotopic substitutions.

The 1536 and 1516 cm^{-1} Positive FTIR Bands Probe the Hybridization State of C(4a). Figure 1 shows several prominent positive difference FTIR bands in the 1000−1600 cm^{-1} range. They include doublets at 1516−1536 and 1372−1378 cm^{-1} and single peaks at 1090, 1298, and 1426 cm^{-1}. Using their strength and expected D/H exchange behavior, we assign the very strong 1516−1536 cm^{-1} doublet to the strong doublet predicted by the calculations in the 1540−1604 cm^{-1} range (bands IV and V, Table 1). These modes involve stretchings of the C(10a)═N1 double bond that are symmetric and antisymmetric to stretching of the C(5a)−C(9a) bond and include some N5−H bend and ring I

stretching. In LOV2$^{D}_{450}$, the flavin bands at 1580 and 1550 cm^{-1} are the two vibrational modes involving symmetric and antisymmetric stretching motions of the conjugated N5═C(4a) and C(10a)═N1 double bonds. In the adduct, the C(4a) carbon acquires a nonplanar sp^3 tetrahedral configuration with loss of the N5═C(4a) double bond. Consequently, this coupling is lost, generating the new stretching modes at 1516−1536 cm^{-1}, which now involve coupling of the C(10a)═N1 double bond and the aromatic C(5a)−C(9a) bond. Figure 3D shows the effect of D/H substitution in this spectral region. Calculations predict negligible shifts for both modes, as is observed experimentally for these two positive bands. Using their relative frequencies, intensities, and observed deuterium shift, we tentatively assign the other positive bands as follows: the 1090 cm^{-1} band to band I (see Table 1), the 1298 cm^{-1} band to band IV, the doublet around 1375 cm^{-1} to bands VI and VII, and the 1426 cm^{-1} band to band VIII. Isotopic substitutions at specific positions are required to confirm these assignments.

Both Chromophore and Protein May Contribute to the FTIR Difference Spectrum in the 1640−1750 cm^{-1} Region. This spectral region includes typically strong infrared absorption bands of carbonyl groups, amide carbonyls, protein amide I transitions, protein amide side chains, and carboxylic acid carbonyls. FMN has two carbonyls at C2 and C4 that give rise to two strong IR active bands (weak Raman) in the 1650−1715 cm^{-1} range (*30*). These bands arise from the predominantly symmetric or antisymmetric C2═O and C4═O stretching modes. Both of these modes are coupled to ring III stretching (*25*), and one includes motion of the N3−H group. Substantial structural changes in ring III upon adduct formation are expected to perturb this coupling and hence the carbonyl stretching frequencies.

The C2 and C4 carbonyl shifts upon adduct formation are expected to produce only two positive and two negative bands in this region of the difference FTIR spectrum. The observed changes are more complex, showing at least three negative and four positive bands. The frequencies of the 1711 and 1670 cm^{-1} negative bands are consistent with previous chromophore carbonyl vibrational assignments for FMN (*30*). All three positive bands observed between 1680 and 1730 cm^{-1} are within the lower end of the range predicted for these modes by our normal-mode calculations on the adduct. In FMN, D/H substitution is expected to shift to a lower wavenumber only the antisymmetric mode because of the large N3−H bend involved in this mode. However, all of the bands in this range shift to some extent to lower wavenumbers upon D/H exchange (data not shown). In LOV2, hydrogen bonding of the carbonyls and/or the N3−H group could account for the observation that all carbonyl modes are sensitive to D/H exchange. The adduct has in addition a new exchangeable proton at N5 that participates in vibrational modes of both FMN carbonyls and is therefore expected to contribute to D/H exchange vibrational frequency perturbations as well as provide a new site for hydrogen bonding interactions with protein side chains.

Although arguments can be presented to explain the sensitivity of protein-bound FMN carbonyl bands to D/H substitution, the additional positive and negative bands in this range cannot be assigned solely to the chromophore. Since the 1620−1690 cm^{-1} region is in the range of the protein amide I and side chain carbonyl amide absorption, these bands may reflect perturbation of protein vibrational bands during the LOV2 photocycle (*22*), particularly from those groups involved in hydrogen bonding. Adduct formation requires hydrogen transfer to N5 (*11*, *13*) and some rearrangement of the cysteinyl side chain (*17*). Our model (*11*) proposes that such intramolecular proton transfer occurs from a protein residue in the vicinity of N5. The additional bands in this region with their strong sensitivity to D/H exchange may reflect changes in the environment caused by this proton transfer reaction.

ACKNOWLEDGMENT

We are grateful to Dr. John M. Christie for extensive technical guidance in preparation of the LOV domain samples used and also for very helpful discussions and critical reading of the manuscript. We are also grateful to Dr. Donald Bivin and Dr. Grant Merrill for assistance in preliminary normal-mode calculations.

REFERENCES

1. Briggs, W. R., Beck, C. F., Cashmore, A. R., Christie, J. M., Hughes, J., Jarillo, J. A., Kagawa, T., Kanegae, H., Liscum, E., Nagatani, A., Okada, K., Salomon, M., Rüdiger, W., Sakai, T., Takano, M., Wada, M., and Watson, J. C. (2001) *Plant Cell 13*, 993−997.
2. Christie, J. M., and Briggs, W. R. (2001) *J. Biol. Chem. 276*, 11457−11460.
3. Kagawa, T., Sakai, T., Suetsugu, N., Oikawa, K., Ishiguro, S., Kato, T., Tabata, S., Okada, K., and Wada, M. (2001) *Science 291*, 2138−2141.
4. Jarillo, J. A., Gabrys, H., Capel, J., Alonso, J. M., Ecker, J. R., and Cashmore, A. R. (2001) *Nature 410*, 952−954.
5. Sakai, T., Kagawa, T., Kasahara, M., Swartz, T. E., Christie, J. M., Briggs, W. R., Wada, M., and Okada, K. (2001) *Proc. Natl. Acad. Sci. U.S.A. 98*, 6969−6974.
6. Christie, J. M., Reymond, P., Powell, G. K., Bernasconi, P., Raibekas, A. A., Liscum, E., and Briggs, W. R. (1998) *Science 282*, 1698−1701.
7. Kinoshita, T., Doi, M., Suetsugu, N., Kagawa, T., Wada, M., and Shimazaki, K. (2001) *Nature 414*, 656−660.
8. Taylor, B. L., and Zhulin, I. B. (1999) *Microbiol. Mol. Biol. Rev. 63*, 479−506.
9. Christie, J. M., Salomon, M., Nozue, K., Wada, M., and Briggs, W. R. (1999) *Proc. Natl. Acad. Sci. U.S.A. 96*, 8779−8783.
10. Salomon, M., Christie, J. M., Knieb, E., Lempert, U., and Briggs, W. R. (2000) *Biochemistry 39*, 9401−9410.
11. Swartz, T. E., Corchnoy, S. B., Christie, J. M., Lewis, J. W., Szundi, I., Briggs, W. R., and Bogomolni, R. A. (2001) *J. Biol. Chem. 276*, 36493−36500.
12. Song, P. S. (1968) *Photochem. Photobiol. 7*, 311−313.
13. Crosson, S., and Moffat, K. (2001) *Proc. Natl. Acad. Sci. U.S.A. 98*, 2995−3000.
14. Kasahara, M., Swartz, T. E., Olney, M. A., Onodera, A., Mochizuki, N., Fukuzawa, H., Asamizu, E., Tabata, S., Kanegae, H., Takano, M., Christie, J. M., Nagatani, A., and Briggs, W. R. (2002) *Plant Phys.* (in press).
15. Miller, S. M., Massey, V., Ballou, D., Williams, C. H., Jr., Distefano, M. D., Moore, M. J., and Walsh, C. T. (1990) *Biochemistry 29*, 2831−2841.
16. Salomon, M., Eisenreich, W., Durr, H., Schleicher, E., Knieb, E., Massey, V., Rudiger, W., Muller, F., Bacher, A., and Richter, G. (2001) *Proc. Natl. Acad. Sci. U.S.A. 98*, 12357−12361.
17. Crosson, S., and Moffat, K. (2002) *Plant Cell 14*, 1−9.
18. Xie, A., Kelemen, L., Hendriks, J., White, B. J., Hellingwerf, K. J., and Hoff, W. D. (2001) *Biochemistry 40*, 1510−1517.
19. Spiro, T. G. (1987) *Biological applications of Raman spectroscopy*, Wiley, New York.

20. Frisch, M. J., Trucks, G. W., Schlegel, H. B., Scuseria, G. E., Robb, M. A., Cheeseman, J. R., Zakrzewski, V. G., Montgomery, J. A., Jr., Stratmann, R. E., Burant, J. C., Dapprich, S., Millam, J. M., Daniels, A. D., Kudin, K. N., Strain, M. C., Farkas, O., Tomasi, J., Barone, V., Cossi, M., Cammi, R., et al. (1998) *Gaussian 98*, revision A.10, Gaussian, Pittsburgh, PA.
21. Scott, A. P., and Radom, L. (1996) *J. Phys. Chem. 100*, 16502−16513.
22. Braiman, M. S., and Rothschild, K. J. (1988) *Annu. Rev. Biophys. Chem. 17*, 541−570.
23. Heberle, J., Kottke, T., Dick, B., and Hegemann, P. (2002) *Biophys. J. 82*, 517a.
24. Nishina, Y., Shiga, K., Horiike, K., Tojo, H., Kasai, S., Yanase, K., Matsui, K., Watari, H., and Yamano, T. (1980) *J. Biochem. 88*, 403−409.
25. Abe, M., and Kyogoku, Y. (1987) *Spectrochim. Acta, Part A 43*, 1027−1038.
26. Bowman, W. D., and Spiro, T. G. (1981) *Biochemistry 20*, 3313−3318.
27. Schmidt, J., Coudron, P., Thompson, A. W., Watters, K. L., and McFarland, J. T. (1983) *Biochemistry 22*, 76−84.
28. Kitagawa, T., Nishina, Y., Kyogoku, Y., Yamano, T., Ohishi, N., Takai-Suzuki, A., and Yagi, K. (1979) *Biochemistry 18*, 1804−1808.
29. Zheng, Y., Dong, J., Palfey, B. A., and Carey, P. R. (1999) *Biochemistry 38*, 16727−16732.
30. Abe, M., Kyogoku, Y., Kitagawa, T., Kawano, K., Ohishi, N., Takai-Suzuki, A., and Yagi, K. (1986) *Spectrochim. Acta, Part A 42*, 1059−1068.

BI025861U